



MŚJŚLewczuk<sup>74</sup> TŚLueck<sup>74</sup> IŚMŚNugeł<sup>74</sup> JŚMŚRondy<sup>74</sup> RŚJŚSobiechowski<sup>74</sup> NŚTasneć<sup>74</sup> TŚJŚGershon<sup>75</sup>  
PŚFŚHarris<sup>75</sup> TŚEŚLatha<sup>75</sup> HŚRŚBaron<sup>76</sup> SŚDał<sup>76</sup> YŚPa<sup>76</sup> RŚPrepot<sup>76</sup> and SŚLŚWu<sup>76</sup>  
(The BABAR Collaboration)

- <sup>1</sup>Laboratoire d'Annecy-le-Vieux de Physique des Particules (LAPP),  
Université de Savoie, CNRS/IN2P3, F-74941 Annecy-Le-Vieux, France
- <sup>2</sup>Universitat de Barcelona, Facultat de Física, Departament ECM, E-08028 Barcelona, Spain
- <sup>3</sup>INFN Sezione di Bari<sup>a</sup>; Dipartimento di Fisica, Università di Bari<sup>b</sup>, I-70126 Bari, Italy
- <sup>4</sup>University of Bergen, Institute of Physics, N-5007 Bergen, Norway
- <sup>5</sup>Lawrence Berkeley National Laboratory and University of California, Berkeley, California 94720, USA
- <sup>6</sup>Ruhr Universität Bochum, Institut für Experimentalphysik 1, D-44780 Bochum, Germany
- <sup>7</sup>University of British Columbia, Vancouver, British Columbia, Canada V6T 1Z1
- <sup>8</sup>Brunel University, Uxbridge, Middlesex UB8 3PH, United Kingdom
- <sup>9</sup>Budker Institute of Nuclear Physics SB RAS, Novosibirsk 630090<sup>a</sup>,  
Novosibirsk State University, Novosibirsk 630090<sup>b</sup>,  
Novosibirsk State Technical University, Novosibirsk 630092<sup>c</sup>, Russia
- <sup>10</sup>University of California at Irvine, Irvine, California 92697, USA
- <sup>11</sup>University of California at Riverside, Riverside, California 92521, USA
- <sup>12</sup>University of California at Santa Barbara, Santa Barbara, California 93106, USA
- <sup>13</sup>University of California at Santa Cruz, Institute for Particle Physics, Santa Cruz, California 95064, USA
- <sup>14</sup>California Institute of Technology, Pasadena, California 91125, USA
- <sup>15</sup>University of Cincinnati, Cincinnati, Ohio 45221, USA
- <sup>16</sup>University of Colorado, Boulder, Colorado 80309, USA
- <sup>17</sup>Colorado State University, Fort Collins, Colorado 80523, USA
- <sup>18</sup>Technische Universität Dortmund, Fakultät Physik, D-44221 Dortmund, Germany
- <sup>19</sup>Technische Universität Dresden, Institut für Kern- und Teilchenphysik, D-01062 Dresden, Germany
- <sup>20</sup>Laboratoire Leprince-Ringuet, Ecole Polytechnique, CNRS/IN2P3, F-91128 Palaiseau, France
- <sup>21</sup>University of Edinburgh, Edinburgh EH9 3JZ, United Kingdom
- <sup>22</sup>INFN Sezione di Ferrara<sup>a</sup>; Dipartimento di Fisica e Scienze della Terra, Università di Ferrara<sup>b</sup>, I-44122 Ferrara, Italy
- <sup>23</sup>INFN Laboratori Nazionali di Frascati, I-00044 Frascati, Italy
- <sup>24</sup>INFN Sezione di Genova<sup>a</sup>; Dipartimento di Fisica, Università di Genova<sup>b</sup>, I-16146 Genova, Italy
- <sup>25</sup>Indian Institute of Technology Guwahati, Guwahati, Assam, 781 039, India
- <sup>26</sup>Harvard University, Cambridge, Massachusetts 02138, USA
- <sup>27</sup>Universität Heidelberg, Physikalisches Institut, D-69120 Heidelberg, Germany
- <sup>28</sup>Humboldt-Universität zu Berlin, Institut für Physik, D-12489 Berlin, Germany
- <sup>29</sup>Imperial College London, London, SW7 2AZ, United Kingdom
- <sup>30</sup>University of Iowa, Iowa City, Iowa 52242, USA
- <sup>31</sup>Iowa State University, Ames, Iowa 50011-3160, USA
- <sup>32</sup>Physics Department, Jazan University, Jazan 22822, Kingdom of Saudia Arabia
- <sup>33</sup>Johns Hopkins University, Baltimore, Maryland 21218, USA
- <sup>34</sup>Laboratoire de l'Accélérateur Linéaire, IN2P3/CNRS et Université Paris-Sud 11,  
Centre Scientifique d'Orsay, F-91898 Orsay Cedex, France
- <sup>35</sup>Lawrence Livermore National Laboratory, Livermore, California 94550, USA
- <sup>36</sup>University of Liverpool, Liverpool L69 7ZE, United Kingdom
- <sup>37</sup>Queen Mary, University of London, London, E1 4NS, United Kingdom
- <sup>38</sup>University of London, Royal Holloway and Bedford New College, Egham, Surrey TW20 0EX, United Kingdom
- <sup>39</sup>University of Louisville, Louisville, Kentucky 40292, USA
- <sup>40</sup>Johannes Gutenberg-Universität Mainz, Institut für Kernphysik, D-55099 Mainz, Germany
- <sup>41</sup>University of Manchester, Manchester M13 9PL, United Kingdom
- <sup>42</sup>University of Maryland, College Park, Maryland 20742, USA
- <sup>43</sup>Massachusetts Institute of Technology, Laboratory for Nuclear Science, Cambridge, Massachusetts 02139, USA
- <sup>44</sup>McGill University, Montréal, Québec, Canada H3A 2T8
- <sup>45</sup>INFN Sezione di Milano<sup>a</sup>; Dipartimento di Fisica, Università di Milano<sup>b</sup>, I-20133 Milano, Italy
- <sup>46</sup>University of Mississippi, University, Mississippi 38677, USA
- <sup>47</sup>Université de Montréal, Physique des Particules, Montréal, Québec, Canada H3C 3J7
- <sup>48</sup>INFN Sezione di Napoli<sup>a</sup>; Dipartimento di Scienze Fisiche,  
Università di Napoli Federico II<sup>b</sup>, I-80126 Napoli, Italy
- <sup>49</sup>NIKHEF, National Institute for Nuclear Physics and High Energy Physics, NL-1009 DB Amsterdam, The Netherlands
- <sup>50</sup>University of Notre Dame, Notre Dame, Indiana 46556, USA
- <sup>51</sup>Ohio State University, Columbus, Ohio 43210, USA
- <sup>52</sup>University of Oregon, Eugene, Oregon 97403, USA
- <sup>53</sup>INFN Sezione di Padova<sup>a</sup>; Dipartimento di Fisica, Università di Padova<sup>b</sup>, I-35131 Padova, Italy

- <sup>54</sup>Laboratoire de Physique Nucléaire et de Hautes Energies, IN2P3/CNRS, Université Pierre et Marie Curie-Paris6, Université Denis Diderot-Paris7, F-75252 Paris, France
- <sup>55</sup>INFN Sezione di Perugia<sup>a</sup>; Dipartimento di Fisica, Università di Perugia<sup>b</sup>, I-06123 Perugia, Italy
- <sup>56</sup>INFN Sezione di Pisa<sup>a</sup>; Dipartimento di Fisica, Università di Pisa<sup>b</sup>; Scuola Normale Superiore di Pisa<sup>c</sup>, I-56127 Pisa, Italy
- <sup>57</sup>Princeton University, Princeton, New Jersey 08544, USA
- <sup>58</sup>INFN Sezione di Roma<sup>a</sup>; Dipartimento di Fisica, Università di Roma La Sapienza<sup>b</sup>, I-00185 Roma, Italy
- <sup>59</sup>Universität Rostock, D-18051 Rostock, Germany
- <sup>60</sup>Rutherford Appleton Laboratory, Chilton, Didcot, Oxon, OX11 0QX, United Kingdom
- <sup>61</sup>CEA, Irfu, SPP, Centre de Saclay, F-91191 Gif-sur-Yvette, France
- <sup>62</sup>SLAC National Accelerator Laboratory, Stanford, California 94309 USA
- <sup>63</sup>University of South Carolina, Columbia, South Carolina 29208, USA
- <sup>64</sup>Southern Methodist University, Dallas, Texas 75275, USA
- <sup>65</sup>Stanford University, Stanford, California 94305-4060, USA
- <sup>66</sup>State University of New York, Albany, New York 12222, USA
- <sup>67</sup>Tel Aviv University, School of Physics and Astronomy, Tel Aviv, 69978, Israel
- <sup>68</sup>University of Tennessee, Knoxville, Tennessee 37996, USA
- <sup>69</sup>University of Texas at Austin, Austin, Texas 78712, USA
- <sup>70</sup>University of Texas at Dallas, Richardson, Texas 75083, USA
- <sup>71</sup>INFN Sezione di Torino<sup>a</sup>; Dipartimento di Fisica, Università di Torino<sup>b</sup>, I-10125 Torino, Italy
- <sup>72</sup>INFN Sezione di Trieste<sup>a</sup>; Dipartimento di Fisica, Università di Trieste<sup>b</sup>, I-34127 Trieste, Italy
- <sup>73</sup>IFIC, Universitat de Valencia-CSIC, E-46071 Valencia, Spain
- <sup>74</sup>University of Victoria, Victoria, British Columbia, Canada V8W 3P6
- <sup>75</sup>Department of Physics, University of Warwick, Coventry CV4 7AL, United Kingdom
- <sup>76</sup>University of Wisconsin, Madison, Wisconsin 53706, USA

We describe searches for  $B$  meson decays to the charmless vector-vector final states  $\omega\omega$  and  $\omega\phi$  with  $471 \times 10^6 B\bar{B}$  pairs produced in  $e^+e^-$  annihilation at  $\sqrt{s} = 10.58$  GeV using the BABAR detector at the PEP-II collider at the SLAC National Accelerator Laboratory. We measure the branching fraction  $\mathcal{B}(B^0 \rightarrow \omega\omega) = (1.2 \pm 0.3_{-0.2}^{+0.3}) \times 10^{-6}$ , where the first uncertainty is statistical and the second is systematic, corresponding to a significance of 4.4 standard deviations. We also determine the upper limit  $\mathcal{B}(B^0 \rightarrow \omega\phi) < 0.7 \times 10^{-6}$  at 90% confidence level. These measurements provide the first evidence for the decay  $B^0 \rightarrow \omega\omega$ , and an improvement of the upper limit for the decay  $B^0 \rightarrow \omega\phi$ .

PACS numbers: 13.25.Hw, 12.15.Hh, 11.30.Er

Charmless decays of  $B$  mesons to two vector mesons have been of significant recent interest, in part because of the unexpectedly small value of the longitudinal polarization component observed in  $B \rightarrow \phi K^*$  decays [1]. The resulting large transverse spin component could be due either to unanticipated large Standard Model (SM) contributions or to non SM effects [4]. Further information and SM constraints on these decays can be obtained from measurements of or limits on the branching fractions of related decays, such as  $B^0 \rightarrow \omega\omega$  and  $B^0 \rightarrow \omega\phi$  [5]. These latter decays are also important because they contain relatively unstudied  $b \rightarrow d$  quark transitions ( $B^0 \rightarrow \omega\omega$  however is expected to be dominated by  $b \rightarrow u$  transitions) and are sensitive to the phase angles  $\alpha$  and  $\gamma$  of the Cabibbo Kobayashi Maskawa quark mixing matrix [6]. Deviations of the observed branching fractions from their SM expectations could provide evidence for physics beyond the SM [5].

Theoretical predictions for the SM branching fractions lie in the range  $(0.5 \text{--} 1.5) \times 10^{-6}$  for  $B^0 \rightarrow \omega\omega$  and  $(0.5 \text{--} 1.5) \times 10^{-6}$  for  $B^0 \rightarrow \omega\phi$  [7]. Previous limits on these

branching fractions are presented in Refs [8, 9]. The results from Ref [8],  $\mathcal{B}(B^0 \rightarrow \omega\omega) < 4.1 \times 10^{-6}$  and  $\mathcal{B}(B^0 \rightarrow \omega\phi) < 1.1 \times 10^{-6}$  are based on about half the final BABAR data sample. In this Letter, we update the results of Ref [9] using the final BABAR dataset and improved analysis techniques [5].

Due to the limited size of the data sample, there is insufficient precision to determine the decay polarization in  $B^0 \rightarrow \omega\omega$  or  $B^0 \rightarrow \omega\phi$ . We therefore integrate over the angular distributions, correcting for detector acceptance and efficiency. The angular distribution is

$$\frac{1}{\Gamma} \frac{d^2\Gamma}{d \cos \theta_{V_1} d \cos \theta_{V_2}} = \frac{9}{4} \left\{ \frac{1}{4} (1 - f_L) \sin^2 \theta_{V_1} \sin^2 \theta_{V_2} - f_L \cos^2 \theta_{V_1} \cos^2 \theta_{V_2} \right\},$$

where  $V_{1,2} = (\{\omega, \omega\} \text{ or } \{\omega, \phi\})$  are vector mesons,  $\theta_{V_{1,2}}$  are helicity angles, and  $f_L$  is the fraction of events with longitudinal spin polarization. For the  $\phi$  meson,  $\theta_\phi$  is the angle in the  $\phi$  rest frame between the positively charged kaon and the boost from the  $B$  rest frame, whereas for

TABLE I: Selection requirements on the invariant mass of  $B$ -daughter intermediate states.

State	Inv. mass (MeV)
$\pi^0$	$120 < m_{\gamma\gamma} < 150$
$\omega$	$740 < m_{\pi\pi\pi} < 820$
$\phi$	$1009 < m_{KK} < 1029$

the angle  $\theta_\omega$  is the angle in the  $\omega$  rest frame between the normal to the  $\omega$  decay plane and the boost from the  $B$  rest frame. For both  $B^0 \rightarrow \omega\omega$  and  $B^0 \rightarrow \omega\phi$ ,  $f_L$  is predicted to be 8% or larger.

The data were collected with the *BABAR* detector at the PEP II asymmetric energy  $e^+e^-$  collider located at the SLAC National Accelerator Laboratory. An integrated luminosity of  $4.9 \text{ fb}^{-1}$ , corresponding to  $N_{B\bar{B}} = (47.2 \pm 0.6) \times 10^6 B\bar{B}$  pairs, was recorded at the  $\Upsilon(4S)$  resonance (center of mass energy  $\sqrt{s} = 10.58 \text{ GeV}$ ). Charged particles are detected, and their momenta measured, by 12 layers of double sided silicon microstrip detectors and a 4 layer drift chamber, both operating in the 1.5 T magnetic field of a superconducting solenoid. We identify photons and electrons using a CsI(Tl) electromagnetic calorimeter. Charged particle identification (PID) is provided by energy loss measurements in the tracking detector and by a ring imaging Cherenkov detector.

We reconstruct the vector meson decays through the  $\omega \rightarrow \pi^+\pi^-\pi^0$  and  $\phi \rightarrow K^+K^-$  channels, with  $\pi^0 \rightarrow \gamma\gamma$ . The minimum laboratory energy (momentum) required for photons (charged kaons) is 5 MeV (2.5 MeV). There is no specific minimum momentum requirement for charged pions but they generally respect  $p_T > 5 \text{ MeV}$ . Charged pion and kaon candidates are rejected if their PID signature satisfies tight consistency with protons or electrons, and the kaons must have a kaon signature, while the pions must not. We require all charged particle products associated with the  $B$  meson candidate decay to be consistent with having originated at a common vertex.

We apply the invariant mass requirements listed in Table I for the  $\pi^0$ ,  $\omega$ , and  $\phi$  mesons. After selection, the  $\pi^0$  is constrained to its nominal mass, which improves the  $\omega$  mass resolution. The restrictions on the  $\omega$  and  $\phi$  meson masses are loose enough to incorporate sideband regions.

A  $B$  meson candidate is characterized kinematically by the energy substituted mass  $m_{ES} = \sqrt{(\frac{1}{2}s - \mathbf{p}_0 \cdot \mathbf{p}_B)^2 / E_0^{*2} - \mathbf{p}_B^2}$  and the energy difference  $\Delta E = E_B^* - \frac{1}{2}\sqrt{s}$ , where  $(E_0, \mathbf{p}_0)$  and  $(E_B, \mathbf{p}_B)$  are the four momenta of the  $\Upsilon(4S)$  and the  $B$  candidate, respectively, and the asterisk denotes the  $\Upsilon(4S)$  rest frame (quantities without asterisks are measured in the laboratory frame). For correctly reconstructed signal candidates,  $\Delta E$  and  $m_{ES}$  peak at values of

zero and  $m_B$ , respectively, with resolutions of about 1 MeV and 5 MeV. This signal events for this analysis mostly fall in the regions  $|\Delta E| \leq 0.2 \text{ GeV}$  and  $5.7 \leq m_{ES} \leq 5.9 \text{ GeV}$ . To incorporate sideband regions, we require  $|\Delta E| \leq 0.5 \text{ GeV}$  and  $5.4 \leq m_{ES} \leq 5.9 \text{ GeV}$ . The average number of candidates found per selected event is 1.5 for  $B^0 \rightarrow \omega\phi$  decays and 1.8 for  $B^0 \rightarrow \omega\omega$  decays. We choose the candidate with the smallest  $\chi^2$  value constructed from the deviations of the  $\omega$  and  $\phi$  resonance masses from their nominal values.

Backgrounds arise primarily from random combinations of particles in continuum events ( $e^+e^- \rightarrow q\bar{q}$ , with  $q = u, d, s, c$ ). We reduce this background by using the angle  $\theta_T$  in the  $\Upsilon(4S)$  rest frame between the thrust axis  $\mathbf{A}$  of the  $B$  candidate and the thrust axis of the other charged and neutral particles in the event. The distribution of  $|\cos\theta_T|$  is sharply peaked near 1 for  $q\bar{q}$  jet pairs, and nearly uniform for  $B$  meson decays. We require  $|\cos\theta_T| < 0.9$  for  $B^0 \rightarrow \omega\phi$  and  $|\cos\theta_T| < 0.8$  for  $B^0 \rightarrow \omega\omega$ .

We employ a maximum likelihood fit, described below, to determine the signal and background yields. For the purposes of this fit, we construct a Fisher discriminant  $\mathcal{F}$  that combines four variables defined in the  $\Upsilon(4S)$  frame: the polar angles with respect to the beam axis of the  $B$  meson momentum and  $B$  thrust axis, and the zeroth and second angular moments  $L_0$  and  $L_2$  of the energy flow about the  $B$  thrust axis. The moments are defined by  $L_j = \sum_i p_i \times |\cos\theta_i|^j$ , where  $\theta_i$  is the angle with respect to the  $B$  thrust axis of a charged or neutral particle,  $p_i$  is its momentum, and the sum excludes the  $B$  candidate daughters.

From simulated event samples produced with Monte Carlo (MC) event generators, we identify the most important backgrounds that arise from other  $B\bar{B}$  decay modes. Most of the  $B\bar{B}$  background does not peak in  $m_{ES}$  or  $\Delta E$  and is grouped with continuum events into a ‘‘combinatoric’’ background category. Other  $B\bar{B}$  decay modes, such as  $B^0 \rightarrow \omega\omega$ ,  $B^0 \rightarrow \omega\phi$ ,  $B^0 \rightarrow \omega\rho$ ,  $B^0 \rightarrow \omega\eta$ , etc., peak in  $m_{ES}$  and/or  $\Delta E$  and are referred to as ‘‘peaking’’ backgrounds. All peaking modes are grouped together into a single background component, with a broad peak centered at negative values of  $\Delta E$ , and which is fitted in data simultaneously with the signal and combinatoric background components.

We obtain signal and background yields from extended unbinned maximum likelihood fits with input observables  $\Delta E$ ,  $m_{ES}$ ,  $\mathcal{F}$ , and, for the vector meson  $V = \omega$  or  $\phi$ , the mass  $m_V$  and the cosine of the helicity angle  $\cos\theta_V$ . For each  $\omega$  meson, there is an additional helicity angle input observable,  $\cos\Phi$ , provided by the polar angle, with respect to the  $\omega$  flight direction, of the  $\pi^0$  in the  $\pi^+\pi^-$  rest frame. This angle is uncorrelated with the other input observables and has a distribution that is proportional to  $\sin^2\Phi_\omega$  for signal. For background, the

angular distribution is nearly flat in  $\cos\theta$ , and its deviation from flatness is parameterized by separate third order polynomials for combinatoric and for peaking  $B\bar{B}$  backgrounds. For each event  $i$  and component  $j$  (signal, combinatoric background, peaking  $B\bar{B}$  background) we define the probability density function (PDF)

$$\mathcal{P}_j^i = \mathcal{P}_j(m_{\text{ES}}^i) \mathcal{P}_j(\Delta E^i) \mathcal{P}_j(\mathcal{F}^i) \times \mathcal{P}_j(m_{V_1}^i, m_{V_2}^i, \cos\theta_{V_1}^i, \cos\theta_{V_2}^i) \times \mathcal{P}_j(\cos\Phi_{\omega_1}^i) \mathcal{P}_j(\cos\Phi_{\omega_2}^i), \quad (4)$$

where the last of the  $\mathcal{P}_j$  terms is not present for  $B^0 \rightarrow \omega\phi$ . The likelihood function is

$$\mathcal{L} = \frac{e^{-(\sum Y_j)}}{N!} \prod_{i=1}^N \sum_j Y_j \mathcal{P}_j^i, \quad (5)$$

where  $Y_j$  is the event yield for component  $j$  and  $N$  is the number of events in the sample.

For signal events, the PDF factor

$$\mathcal{P}_{\text{sig}}(m_{V_1}^i, m_{V_2}^i, \cos\theta_{V_1}^i, \cos\theta_{V_2}^i)$$

takes the form

$$\mathcal{P}_{1,\text{sig}}(m_{V_1}^i) \mathcal{P}_{2,\text{sig}}(m_{V_2}^i) \mathcal{Q}(\cos\theta_{V_1}^i, \cos\theta_{V_2}^i), \quad (4)$$

where  $\mathcal{Q}$  corresponds to the right hand side of Eq. (4) after modification to account for detector acceptance. For combinatoric background events, the PDF factor is given for each vector meson independently by

$$\mathcal{P}_{\text{cont}}(m_V^i, \cos\theta_V^i) = \mathcal{P}_{\text{peak}}(m_V^i) \mathcal{P}_{\text{peak}}(\cos\theta_V^i) \mathcal{P}_{\text{cont}}(m_V^i) \mathcal{P}_{\text{cont}}(\cos\theta_V^i), \quad (5)$$

distinguishing between genuine resonance ( $\mathcal{P}_{\text{peak}}$ ) and combinatorial ( $\mathcal{P}_{\text{cont}}$ ) components. The background PDFs  $\mathcal{P}_{\text{peak}}(\cos\theta_V^i)$  and  $\mathcal{P}_{\text{cont}}(\cos\theta_V^i)$  are given by separated third order polynomials. For the peaking  $B\bar{B}$  background, we assume that all four mass and helicity angle observables are independent.

To describe the PDFs for signal, we use the sum of two Gaussians for  $\mathcal{P}_{\text{sig}}(m_{\text{ES}})$  and for  $\mathcal{P}_{\text{sig}}(\Delta E)$ . An asymmetric Gaussian is used for  $\mathcal{P}_{\text{sig}}(\mathcal{F})$ , with two half Gaussian distributions (one on the right side of the mean and one on the left side) with different values for the standard deviation, summed with a small additional Gaussian component to account for misreconstructed signal events. The  $m_{V_1}$ ,  $\Delta E$ , and  $\mathcal{F}$  PDFs for peaking  $B\bar{B}$  background have the same functional form as for signal events, but their parameters are determined separately. The genuine resonance components of  $\mathcal{P}_j(m_V)$  are both described by relativistic Breit Wigner distributions, each convolved with the sum of two Gaussians to account for detector resolution, while the combinatoric components of  $\mathcal{P}_j(m_V)$  are described by third order polynomials. For

the combinatoric background category, the  $m_{\text{ES}}$  distribution is described by an ARGUS function  $A(m_{\text{ES}}) \propto x\sqrt{a-x^2} \exp[-\xi(a-x^2)]$  (with  $x \equiv m_{\text{ES}}/E_B^*$ ), the  $\Delta E$  distribution by a second order polynomial, and the  $\mathcal{F}$  distribution by an asymmetric Gaussian summed with an additional Gaussian. The background PDF parameters that are allowed to vary in the fit are the ARGUS function parameter  $\xi$  for  $m_{\text{ES}}$ , the polynomial coefficients describing the combinatorial and the peaking  $B\bar{B}$  components for  $\Delta E$  and  $m_{V_1}$ , and the  $B\bar{B}$  peak position and the two standard deviation parameters of the asymmetric Gaussian for  $\mathcal{F}$ .

For signal events, the PDF parameters are determined from simulation. We study large control samples of  $B \rightarrow D^{(*)}X$  events with similar topology to the signal modes, such as  $B^0 \rightarrow D^- \pi^+$ , to verify the simulated resolutions in  $m_{\text{ES}}$  and  $\Delta E$ . We make small adjustments to the signal PDFs to account for any differences that are found.

In the fit to data, parameters (out of around 20) are allowed to vary for each mode including the yields  $Y_j$  of the signal, total peaking  $B\bar{B}$  background, and total combinatoric background, and ten parameters of the continuum background PDFs. For both modes, we set  $f_L$  to 0.5, a value consistent with theoretical expectation. The event yields with their statistical uncertainties are presented in Table II.

We evaluate possible biases in the signal yields, which might arise as a consequence of neglected correlations between the discriminating variables, by applying our fit to an ensemble of simulated experiments. The numbers of signal and peaking  $B\bar{B}$  background events in these samples are Poisson distributed around the observed values and are extracted randomly from MC samples that include simulation of the detector. The largest of the correlations (approximately 5%) is between the analysis variables  $m_{\text{ES}}$  and  $\Delta E$ . The signal yield bias  $Y_{\text{sig}}^{\text{bias}}$  we find for each mode is provided in Table II.

The resulting branching fractions are calculated as

$$\mathcal{B} = \frac{Y_{\text{sig}} - Y_{\text{sig}}^{\text{bias}}}{\epsilon N_{B\bar{B}}}, \quad (6)$$

where the signal efficiencies  $\epsilon$  are evaluated using MC and data control samples. The total number of  $B\bar{B}$  pairs in data  $N_{B\bar{B}}$  is evaluated using a dedicated analysis.

The systematic uncertainties on the branching fractions are summarized in Table III. The uncertainty attributed to the yield bias correction is taken to be the quadrature sum of two terms: half of the bias correction and the statistical uncertainty on the bias itself. The uncertainties of PDF parameters that are fixed in the fit are evaluated by taking the difference between the respective parameter values determined in fits to simulated and observed  $B \rightarrow D^{(*)}X$  events. Varying the signal PDF parameters within these uncertainties, we estimate yield uncertainties for each mode. Similarly, the uncertainty due

TABLE II: Fitted signal yield  $Y_{\text{sig}}$  and its statistical uncertainty, signal yield bias  $Y_{\text{sig}}^{\text{bias}}$ , peaking  $B\bar{B}$  and combinatoric background yields  $Y_{\text{peak}}$  and  $Y_{\text{comb}}$  and their statistical uncertainties, signal detection efficiency  $\epsilon$  and its statistical uncertainty, daughter branching fraction product  $\prod \mathcal{B}_i$  and its total uncertainty, significance  $S$  (with systematic uncertainties included), measured branching fraction  $\mathcal{B}$  (bold if evidence for signal is seen), and 90% CL upper limit (UL, bold if no evidence) for the  $B^0 \rightarrow \omega\omega$  and  $B^0 \rightarrow \omega\phi$  decay modes.

Mode	$Y_{\text{sig}}$ (events)	$Y_{\text{sig}}^{\text{bias}}$ (events)	$Y_{\text{peak}}$ (events)	$Y_{\text{comb}}$ (events)	$\epsilon$ (%)	$\prod \mathcal{B}_i$ (%)	$S$ ( $\sigma$ )	$\mathcal{B}$ ( $10^{-6}$ )	$\mathcal{B}$ UL ( $10^{-6}$ )
$\omega\omega$	$69.0^{+16.4}_{-15.2}$	7.3	$3810 \pm 260$	$53390 \pm 340$	$14.0 \pm 0.1$	$77.5 \pm 1.2$	4.4	<b><math>1.2 \pm 0.3^{+0.3}_{-0.2}</math></b>	1.9
$\omega\phi$	$-2.8^{+5.7}_{-4.0}$	-2.9	$473^{+84}_{-80}$	$17730^{+160}_{-150}$	$8.7 \pm 0.1$	$43.2 \pm 0.6$	0.0	$0.0^{+0.3}_{-0.2} \pm 0.1$	<b>0.7</b>

TABLE III: Estimated systematic uncertainties on the branching fractions  $\mathcal{B}(B^0 \rightarrow \omega\omega)$  and  $\mathcal{B}(B^0 \rightarrow \omega\phi)$ . Additive and multiplicative uncertainties are independent and are combined in quadrature. Note that only the additive uncertainties are consequential in the case of the  $B^0 \rightarrow \omega\phi$  mode, as essentially zero signal is observed in that mode.

Decay Mode	$B^0 \rightarrow \omega\omega$	$B^0 \rightarrow \omega\phi$
Additive uncertainties (events):		
Fit bias	5.5	2.0
Fit parameters	0.5	0.3
$B\bar{B}$ backgrounds	< 0.1	< 0.1
Total additive (events)	5.5	2.0
Multiplicative uncertainties (%):		
$f_L$ variation	+25.3 -8.3	+18.3 -48.0
Vertex finding efficiency	+5.3 -0.0	+25.0 -50.0
Track finding efficiency	1.0	1.0
$\pi^0$ efficiency	4.2	2.1
Kaon identification	—	4.5
$\cos\theta_T$ cut efficiency	1.3	1.4
Submode branching fractions	1.6	1.5
MC statistics	1.0	1.4
Total number of $B\bar{B}$ in data	0.6	0.6
Total multiplicative (%)	+26.3 -9.7	+31.5 -69.5

to the modeling of the peaking  $B\bar{B}$  background is estimated as the change in the signal yield when the number of peaking  $B\bar{B}$  background events is fixed (to within one standard deviation) of the expectation from simulation. We evaluate an uncertainty related to the constraint that all charged particles in the  $B$  candidate emanate from a common vertex by the change in signal yield when this requirement is removed. The uncertainty associated with  $f_L$  is evaluated by the change relative to the standard result when  $f_L$  is varied between the extreme values of 0.58 (the value of  $f_L$  in  $B \rightarrow \phi K^*$  decays) and 0.85.

Systematic uncertainties associated with the selection efficiency, evaluated with data control samples, are  $0.8\% \times N_t$  and  $0.5\% \times N_\pi$ , where  $N_t$  is the number of tracks and  $N_\pi$  the number of  $\pi^0$  mesons. The uncertainty of  $N_{B\bar{B}}$  is  $0.5\%$ . World averages provide the uncertainties in the  $B$  daughter product branching fractions ( $0.5\%$ ). The uncertainty associated with the requirement on  $\cos\theta_T$  is  $0.5\%$  depending on the decay mode.

Table II also presents the measured branching fractions, total associated uncertainties, and significances. The significance, which we denote in terms of the analogous number of Gaussian standard deviations, is taken as the square root of the difference between the value of  $-\ln\mathcal{L}$  (with systematic uncertainties included) for zero signal events and the value at its minimum. The behavior of  $-\ln\mathcal{L}(\mathcal{B})$  for the two modes is shown in Fig. 1. We find evidence for  $B^0 \rightarrow \omega\omega$  decays at the level of 4.4 standard deviations including systematic uncertainties. For each mode we also quote a 90% CL upper limit, taken to be the branching fraction below which lies 90% of the total of the likelihood integral in the positive branching fraction region. In calculating branching fractions we assume that the decay rates of the  $\Upsilon(4S)$  to  $B^+B^-$  and  $B^0\bar{B}^0$  are equal.

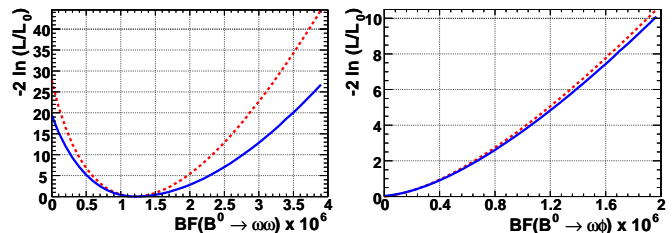


FIG. 1: Distribution of  $-2 \ln(L/L_0)$  (normalized to the maximum likelihood  $L_0$ ) for  $B^0 \rightarrow \omega\omega$  (left) and  $B^0 \rightarrow \omega\phi$  (right) decays. The dashed curves include only statistical uncertainties; the solid curves include systematic uncertainties as well.

Figure 2 presents the data and PDFs projected onto  $m_{ES}$  and  $\Delta E$  for subsamples enriched with signal events via a set of selection criteria on the analysis variables. The selection criteria are  $|m_\omega - m_\omega^{\text{nominal}}| < 5 \text{ MeV}$ ,  $|m_\phi - m_\phi^{\text{nominal}}| < 8 \text{ MeV}$ ,  $\mathcal{F} < 0.5$ ,  $|\cos\Phi_\omega| < 0.5$ , and  $|\cos\theta_T| < 0.8$  with  $|\Delta E| < 0.5 \text{ MeV}$  for the two  $m_{ES}$  plots and  $m_{ES} > 5.74 \text{ GeV}$  for the two  $\Delta E$  plots. These criteria retain 4% of  $B^0 \rightarrow \omega\omega$  ( $B^0 \rightarrow \omega\phi$ ) signal events and in both modes reject over 99% of the background events.

In summary, we have performed searches for  $B^0 \rightarrow \omega\omega$  and  $\omega\phi$  decays. We establish the following branching

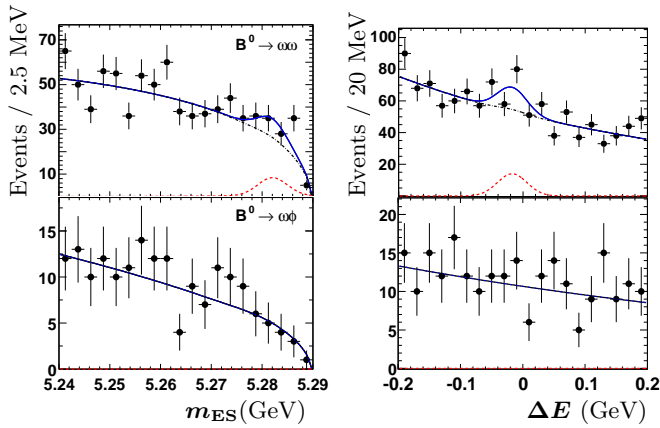


FIG. 2: Projections of  $m_{ES}$  (left) and  $\Delta E$  (right) for a signal-enriched sample of events passing a set of dedicated selection cuts for  $B^0 \rightarrow \omega\omega$  (upper plots), and  $B^0 \rightarrow \omega\phi$  (lower plots). The solid curve gives the total PDF (computed without the variable plotted), the dashed curve is the signal contribution, and the dot-dashed curve is the background contribution, which includes both combinatoric and peaking  $B\bar{B}$  backgrounds.

fraction and upper limit:

$$\mathcal{B}(B^0 \rightarrow \omega\omega) = (0.2 \pm 0.3 \pm 0.2) \times 10^{-6} \quad \text{and}$$

$$\mathcal{B}(B^0 \rightarrow \omega\phi) < 0.7 \times 10^{-6} \quad (9\% \text{ CL}).$$

For the branching fractions, the first uncertainty is statistical and the second is systematic. These results provide the first evidence for  $B^0 \rightarrow \omega\omega$  decays and improve the constraint on the  $B^0 \rightarrow \omega\phi$  branching fraction. Our results are in agreement with theoretical estimates [1, 2].

We are grateful for the excellent luminosity and machine conditions provided by our PEP II colleagues, and for the substantial dedicated effort from the computing organizations that support BABAR. The collaborating institutions wish to thank SLAC for its support and kind hospitality. This work is supported by DOE and NSF (USA), NSERC (Canada), CEA and CNRS INP (France), BMBF and DFG (Germany), INFN (Italy), FOM (The Netherlands), NFR (Norway), MES (Russia), MINECO (Spain), STFC (United Kingdom), BSF (USA), Israel. Individuals have received support from the Marie Curie EIF (European Union) and the A.P.S. Sloan Foundation (USA).

\* Now at the University of Tabuk, Tabuk 71491, Saudi Arabia

† Also with Università di Perugia, Dipartimento di Fisica, Perugia, Italy

‡ Now at Laboratoire de Physique Nucléaire et de Hautes Energies, IN2P3/CNRS, Paris, France

§ Now at the University of Huddersfield, Huddersfield HD1 3DH, UK

¶ Deceased

\*\* Now at University of South Alabama, Mobile, Alabama 36688, USA

†† Also with Università di Sassari, Sassari, Italy

‡‡ Also with INFN Sezione di Roma, Roma, Italy

§§ Now at Universidad Técnica Federico Santa María, Valparaíso, Chile 2390123

- [1] BABAR Collaboration, B. Aubert *et al.*, Phys. Rev. Lett. **91**, 171802 (2003); BABAR Collaboration, B. Aubert *et al.*, Phys. Rev. Lett. **93**, 231804 (2004); BABAR Collaboration, B. Aubert *et al.*, Phys. Rev. Lett. **98**, 051801 (2007); BABAR Collaboration, B. Aubert *et al.*, Phys. Rev. Lett. **99**, 201802 (2007).
- [2] Belle Collaboration, K. F. Chen *et al.*, Phys. Rev. Lett. **91**, 201801 (2003); Belle Collaboration, K. F. Chen *et al.*, Phys. Rev. Lett. **94**, 221804 (2005); Belle Collaboration, M. Prim *et al.*, Phys. Rev. D **88**, 072004 (2013).
- [3] C.W. Bauer *et al.*, Phys. Rev. D **70**, 054015 (2004); P. Colangelo, F. De Fazio, and T.N. Pham, Phys. Lett. B **597**, 291 (2004); A.L. Kagan, Phys. Lett. B **601**, 151 (2004); M. Ladisa *et al.*, Phys. Rev. D **70**, 114025 (2004); H. Y. Cheng, C. K. Chua, and A. Soni, Phys. Rev. D **71**, 014030 (2005); H.-n. Li and S. Mishima, Phys. Rev. D **71**, 054025 (2005); H.-n. Li, Phys. Lett. B **622**, 63 (2005).
- [4] W. Bensalem and D. London, Phys. Rev. D **64**, 116003 (2001); A. K. Giri and R. Mohanta, Phys. Rev. D **69**, 014008 (2004); E. Alvarez *et al.*, Phys. Rev. D **70**, 115014 (2004); C.-H. Chen and C.-Q. Geng, Phys. Rev. D **71**, 115004 (2005); Y.-D. Yang, R. M. Wang and G. R. Lu, Phys. Rev. D **72**, 015009 (2005); P. K. Das and K. C. Yang, Phys. Rev. D **71**, 094002 (2005); C.-H. Chen and C.-Q. Geng, Phys. Rev. D **71**, 115004 (2005); A. K. Giri and R. Mohanta, Eur. Phys. Jour. C **44**, 249 (2005); S. Baek *et al.*, Phys. Rev. D **72**, 094008 (2005); S.-S. Bao *et al.*, Phys. Rev. D **77**, 095004 (2008).
- [5] S. Oh, Phys. Rev. D **60**, 034006 (1999).
- [6] D. Atwood and A. Soni, Phys. Rev. D **59**, 013007 (1998); D. Atwood and A. Soni, Phys. Rev. D **65**, 073018 (2002); H.-W. Huang *et al.*, Phys. Rev. D **73**, 014011 (2006).
- [7] G. Kramer and W.F. Palmer, Phys. Rev. D **45**, 193 (1992); G. Kramer and W.F. Palmer, Phys. Rev. D **46**, 2969 (1992); A. Ali, G. Kramer, and C.-D. Lü, Phys. Rev. D **58**, 094009 (1998); A. Ali, G. Kramer, and C.-D. Lü, Phys. Rev. D **59**, 014005 (1998); Y.H. Chen *et al.*, Phys. Rev. D **60**, 094014 (1999); H.-Y. Cheng and K.C. Yang, Phys. Lett. B **511**, 40 (2001).
- [8] CLEO Collaboration, T. Bergfeld *et al.*, Phys. Rev. Lett. **81**, 272 (1998).
- [9] BABAR Collaboration, B. Aubert *et al.*, Phys. Rev. D **74**, 051102 (2006).
- [10] Y. Li and C.-D. Lü, Phys. Rev. D **73**, 014024 (2006); H.-Y. Cheng and C.-K. Chua, Phys. Rev. D **80**, 114008 (2009).
- [11] BABAR Collaboration, B. Aubert *et al.*, Nucl. Instrum. Methods Phys. Res., Sect. A **729**, 615 (2013); BABAR Collaboration, B. Aubert *et al.*, Nucl. Instrum. Methods Phys. Res., Sect. A **479**, 1 (2002).
- [12] BABAR Collaboration, J. P. Lees *et al.*, Nucl. Instrum. Methods Phys. Res., Sect. A **726**, 203 (2013).
- [13] Particle Data Group, J. Beringer *et al.*, Phys. Rev. D **86**, 010001 (2012).
- [14] S. Brandt *et al.*, Phys. Lett. **12**, 57 (1964).
- [15] R. A. Fisher, Ann. Eugenics **7**, 179 (1936).
- [16] The BABAR detector Monte Carlo simulation is based

- on the EVTGEN event generator: D. Lange, Nucl. Instrum. Methods Phys. Res., Sect. A **462**, 152 (2001), and GEANT4 detector response simulation: S. Agostinelli *et al.*, Nucl. Instrum. Methods Phys. Res., Sect. A **506**, 250 (2003).
- [17] ARGUS Collaboration, H. Albrecht *et al.*, Phys. Lett. B **241**, 278 (1990).
- [18] G. D. McGregor, SLAC-R-912, [arXiv:0812.1954](https://arxiv.org/abs/0812.1954) [[hep-ex](https://arxiv.org/archive/hep)] (2008).
- [19] T. Allmendinger *et al.*, Nucl. Instrum. Methods Phys. Res., Sect. A **704**, 44 (2013).